Applied Catalysis A: General 353 (2009) 17–23

Contents lists available at ScienceDirect

Applied Catalysis A: General

journal homepage: www.elsevier.com/locate/apcata

LCO hydrotreating with Mo-Ni and W-Ni supported on nano- and micro-sized zeolite beta

Lianhui Ding [a,*], Ying Zheng [b], Hong Yang [a], Rahimi Parviz [a]

[a] National Centre for Upgrading Technology, CANMET, Devon, AB T9G 1A8 Canada
[b] Department of Chemical Engineering, University of New Brunswick, PO Box 4400, Fredricton, NB E3B 5A3 Canada

ARTICLE INFO

Article history:
Received 12 August 2008
Received in revised form 8 October 2008
Accepted 11 October 2008
Available online 28 October 2008

Keywords:
Nano-sized zeolite
Zeolite beta
Hydrotreating
LCO

ABSTRACT

The effect of zeolite beta particle size on the HDS, HDN, and HDA activities of LCO hydrotreating was investigated on Mo-Ni and W-Ni supported on nano- and micro-sized zeolite beta hydrotreating catalysts. The catalysts were characterized by XRD, BET, TEM, and XPS, and evaluated with an autoclave using real LCO as feed. It was concluded that, with the Mo-Ni catalysts, the catalyst containing nano-sized zeolite beta particles had similar hydrogenation activity as the one containing micro-sized (conventional) particles; with the W-Ni catalyst, the nano-sized zeolite catalyst presented higher HDS, HDN, and HDA activities as expected. Higher liquid yields could be achieved by using the W-Ni and Mo-Ni nano-sized zeolite catalysts.

1. Introduction

As a consequence of reductions in the yields of straight-run diesel fractions associated with the declining quality of crude oil worldwide, more low-quality feeds with higher sulfur and aromatics contents, such as light cycle oil (LCO) from fluid catalytic cracking units, have to be blended into the streams to hydrotreaters to meet market demand for diesel fuel. Conventional hydrotreating catalysts and processes cannot cost-effectively reduce the sulfur and aromatics with such feeds to meet increasingly stringent environmental regulations [1]. Novel catalysts with deeper hydrodesulfurization (HDS) and hydrodearomatization (HDA) activities need to be developed.

It has been proved that HDS and HDA activities can be significantly improved by increasing the acidity of catalysts [1–6]. Zeolite beta was believed to be one of the most suitable acidity components for use in hydrotreating LCO because of its appropriate pore structure and acidity [5]. However, its interconnected 12-membered ring channels, with pore openings of 0.55 nm × 0.55 nm and 0.76 nm × 0.64 nm, make it difficult for the large molecules present in oil fractions to diffuse to the inner surface where most of the reaction sites are located.

An effective way of reducing or eliminating undesired diffusion limitations on the reaction rate is to reduce the crystal sizes of the zeolites [7–9]. Meanwhile, reducing the crystal size to the nano scale produces substantial changes in the physicochemical properties of the zeolite. Nano-sized zeolite beta crystals were reported to exhibit higher catalytic activity, a lower rate of catalyst deactivation, and higher product quality than conventional (micro-sized) microcrystalline beta material [8,10–16]. Camblor et al. [10] revealed that the catalyst containing the nanocrystalline zeolite beta (particle size 10 nm) was more active in mild hydrocracking, HDS, and hydrodenitrogenation (HDN) than that containing larger crystals (200 nm), despite the latter zeolite having more Brønsted acid sites. They attributed the results to the higher mesoporosity of the nanocrystalline sample and a greater number of external acid sites that are easily accessible by the large molecules present in the gas oil feed. As for the selectivity, the catalyst containing nano-sized zeolite produced fewer gases and more middle distillates, which indicates that diffusion of the molecules is strongly favored in the very small crystallines of the zeolites, and the secondary cracking of the intermediate product molecules is lessened or eliminated. Landau et al. [8] also proved that the reduction of the zeolite crystal size to the nanoscale range increased the rate constant and the effectiveness factor in HVGO hydrocracking approximately two-fold. When the crystal size of zeolite beta was smaller than 50 nm, the diffusion limitations became insignificant. The greatly increased external specific surface area and high fraction of acid sites provide the active sites for the molecules that are too big to enter the pores of zeolites. 1,3,5-triisopropylbenzene (diameter >9.0 Å) cannot penetrate the cavities of Faujasites zeolites (pore opening 7.4 Å), and is therefore taken as a

* Corresponding author. Tel.: +1 780 9878713 fax: +1 780 987 5349.
E-mail address: lding@nrcan.gc.ca (L. Ding).

0926-860X/$ – see front matter.
doi:10.1016/j.apcata.2008.10.023

convenient probe molecule to simulate the cracking of heavy gas oil molecules on the external surface of the zeolite. The cracking of 1,3,5-triisopropylbenzene over two Y zeolites of 63- and 193-nm crystallite sizes revealed that much greater activity was obtained with the smaller crystallite sample [12].

The most common combinations of hydrogenation metals in hydroprocessing catalysts are Mo-Co, Mo-Ni, and W-Ni. Mo-Co catalysts have higher HDS activity but lower HDN and HDA activities than Mo-Ni and W-Ni catalysts. Of the three combinations, W-Ni exhibits the highest HDA and HCR activities [17]. When HDS, HDN, and HDA activities need to be simultaneously enhanced, Mo-Ni and W-Ni catalysts are preferred.

Comparisons between Mo-Ni and W-Ni hydrotreating catalysts supported on nano- and micro-sized zeolite beta particles are not as well-documented. Accordingly, the purpose of this work is to investigate the effect of the particle sizes of zeolite beta, especially in the nano-size regime, on the hydrogenation performances of the nano- and micro-sized zeolite beta catalysts and to compare the effects of Mo-Ni and W-Ni combinations in hydrotreating LCO.

2. Experimental

2.1. Catalyst preparation

Micro-sized (0.5 μm) and nano-sized (30 nm) zeolite Na-beta were synthesized by the method described in the literature [18]. The synthesized zeolite Na-beta was ion-exchanged with 1.0 M NH_4NO_3 aqueous solution three times at 368 K for 1 h and then dried at 373 K overnight. The dried zeolite powder samples were treated under 0.1 MPa "self-steam" pressure in an autoclave at 823 K for 1 h. The above hydrothermally treated zeolite beta was mixed with large-pore alumina (Sasol PURALOX TH100/150, pore volume 0.96 mL/g, specific surface area 201.6 m^2/g), MoO_3, nickel nitrate hexahydrate, and binder (partially acid-peptized alumina, SASOL, CATAPAL B), extruded to form cylindrically shaped extrudate, dried at 383 K overnight, and then calcined in air at 773 K for 4 h. The catalysts containing nano-sized and micro-sized beta particles were designated as MoNi/NB and MoNi/MB, respectively. The nano-sized and micro-sized zeolite beta was mixed with aforementioned large-pore alumina and binder, extruded to form cylindrically shaped extrudate, dried at 383 K overnight, and then calcined in air at 823 K for 4 h to form the supports. The WNi catalysts were prepared by co-impregnation of the above supports using the incipient wetness method with an aqueous solution of the appropriate amounts of nickel nitrate hexahydrate [$Ni(NO_3)_2{\cdot}6H_2O$] and ammonium metatungstate [$(NH_4)_6H_2W_{12}O_{40}$], dried at 383 K overnight, and calcinated at 773 K for 4 h. The catalysts containing nano-sized and micro-sized beta particles were designated as WNi/NB and WNi/MB, respectively. The catalyst compositions are given in Table 1.

Table 1
Catalyst compositions (wt%).

Catalyst	MoNi/NB	MoNi/MB	WNi/NB	W-Ni/MB
Size of zeolite	Nano-beta	Micro-beta	Nano-beta	Micro-beta
WO_3			24	24
MoO_3	15	15		
NiO	5	5	5	5
Zeolite beta	15	15	15	15
Large-pore alumina	45	45	36	36
Binder	20	20	20	20

2.2. Catalyst characterization

X-ray photoelectron spectroscopy (XPS) of the samples was performed using a VG Microtech MultiLab ESCA 2000 system with a CLAM4 hemispherical analyzer. The source was non-monochromatized Mg Kα X-rays at 1253.6 eV (15 kV, 20 mA). In order to sample a greater depth, photoelectron detection perpendicular to the sample surface was chosen. The high-resolution C1s spectra of the adventitious hydrocarbon (at 284.5 eV) on the sample surfaces were recorded before and after each measurement and used as a reference for charge correction. Quantitative information on surface composition was obtained from integrated peak intensities and atomic sensitivity factors using the Advantage data acquisition and processing software supplied by Thermo VG Scientific. Peak fittings of all spectra were performed using the Shirley background correction and Gaussian–Lorentzian curve synthesis. The spatial resolution for surface mapping is 100 μm. The energy resolution is 10 meV. The detection limit is 0.1 atom percent. The binding energy values are quoted with a precision of ±0.15 eV. To prepare the sulfided W-Ni or Mo-Ni catalyst for XPS, a 2-g catalyst sample was pre-sulfided in a 1-L autoclave with 3 mL DMDS at 593 K for 2 h and at 633 K for another 2 h under an initial hydrogen pressure of 3.4 MPa. The sulfided catalyst was quickly sealed in an Ampule bottle under the protection of nitrogen. Before XPS analysis, the sample was handled in a glove box filled with helium, and then quickly transferred into the XPS machine to avoid exposure to air.

The nitrogen adsorption measurements (BET) were performed on a Quantachrome Autosorb-1. Before adsorption, the samples were calcined at 823 K for 16 h. Powder samples of 30–40 mg of powder samples were degassed in a sample preparation station under 473 K and 1.33×10^{-3} Pa for 15 h, then switched to the analysis station for adsorption and desorption under liquid nitrogen at 77 K with an equilibrium time of 2 min. Specific surface area was calculated using a multipoint BET equation with a linear region in the P/Po range of 0.05–0.35. Pore volume was calculated from the maximum adsorption amount of nitrogen at P/Po = 0.99.

The crystallinity and phase purity of solid products were characterized by powder X-ray diffraction (XRD) using a Bruker AXS D8 ADVANCE instrument. Cu Kα radiation is provided by a graphite monochromator. The step time is 0.5 s and the step size is 0.02°/step. For zeolite beta, the crystallinity was calculated through comparison of the area under the most intense diffraction peak (3 0 2) at 22.8° (2θ) to that of reference zeolite beta, whose crystallinity was considered to be 100%.

The particle sizes were determined by transmission electron microscopy (TEM) on a JEOL 2010 STEM operated at 200 keV. The spectra were collected using an EDAX Genesis 4000 system. The catalyst samples were sulfided by the same method as described in XPS analysis. Instead of sealing the sulfided sample in an Ampule bottle, 100% ethanol was quickly added to the vial that contained the sulfided sample. Samples for TEM tests were prepared by the drop method. EDX was used to identify the surface MoS_2 and WS_2 species. For WS_2 or MoS_2 on the catalysts, the average number of layers per slab and average length of slabs were calculated from the measurement of about 300 crystallites with the following equations.

$$\text{Average slab length } \overline{L} = \frac{\sum_{i=1}^{n} n_i l_i}{\sum_{i=1}^{n} n_i}$$

and

$$\text{Average number of layers } \overline{N} = \frac{\sum_{i=1}^{n} n_i N_i}{\sum_{i=1}^{n} n_i}$$

where l_i is the length of the slab, n_i the number of the particles with the l_i length or N_i layers, and N_i the number of layers in the particle

i. On the basis of 7–9 TEM images taken at different areas of one sample, the WS_2 slab length was measured manually using the TEM supported software and the average length of the WS_2 slab was calculated. The experimental error for the slab length was ±0.5 nm. The standard deviations of the slab lengths for MoNi and WNi catalysts were about 4.0 nm and 11 nm respectively. The standard deviations of the layer numbers for MoNi/MB, MoNi/NB, WNi/MB, and WNi/NB were 1.63, 0.56, 2.82, and 2.36 respectively.

2.3. Catalyst performance evaluation

The catalyst activity evaluation was carried out in a 1-L stirred autoclave reactor (Autoclave Engineers Division of Snap-tite, Inc. Eze-Seal stirred reactor). The properties of LCO are listed in Table 2. Twenty grams of the catalyst were loaded in the catalyst basket in the reactor. The reactor was repeatedly evacuated and refilled with hydrogen to replace the air in the autoclave. Five millilitres of sulfiding agent, dimethly disulfide (DMDS), were added to the reactor. The theoretical calculation and experimental results on DMDS decomposition demonstrated that 5 mL of DMDS is sufficient to sulfide 20 g catalyst. Prior to heating the reactor, the reactor was pressurized to 3.4 MPa. The catalyst was sulfided in situ at 593 K for 2 h and at 633 K for another 2 h. After the sulfidation, LCO was charged into the batch autoclave reactor through a feed charging tank mounted on the top of the reactor. The reactor was pressurized to 4.8 MPa, and temperature was increased to 648 K at a rate of 3 K/min under 1000-rpm stirring. When the temperature reached the set temperature (648 K), the hydrogen pressure was adjusted to 6.8 MPa and maintained for 1 h under stirring. After reaction, the liquid product was collected and analyzed. The nitrogen, sulfur, and aromatics were analyzed in terms of ASTM D4629, ASTM D4294, and ASTM D6591, respectively. The boiling ranges of LCO and liquid products were measured with simulated distillation by gas chromatography. The HDS, HDN, and HDA activities of the catalysts were determined by the equation:

$$\text{Activity} = \frac{x_F - x_P}{x_F} \times 100\%$$

where x_F and x_P stand for the sulfur, nitrogen, and saturate (from hydrocarbon composition analysis) contents in feed and product, respectively.

3. Results and discussion

3.1. Textural properties of the catalysts

The textural properties of the starting zeolite beta, hydrothermally treated zeolites, and four oxide catalysts prepared from the corresponding treated zeolites are summarized in Table 3. Due to the existence of mesopores and interparticulate space [18,19], two nano-sized Na-betas and their corresponding hydrothermally treated zeolites exhibited the higher pore volumes and surface areas than the micro-size ones, as expected. Hydrothermal treatment led to less pore volume decrease (from 0.86 mL/g to 0.81 mL/g) and more specific surface area decrease (734 m^2/g to 504 m^2/g) for the nano-sized zeolite beta than for the micro-sized zeolite (0.63 mL/g to 0.46 mL/g in pore volume, 498 m^2/g to 432 m^2/g in specific surface area). However, when the final catalysts were formed, MoNi/NB and MoNi/MB catalysts and WNi/NB and WNi/MB catalysts showed quite similar pore volumes, surface areas, and pore sizes irrespective of their original nano- or micro-sized zeolites. Compared with MoNi catalysts, WNi catalysts had lower pore volumes and surface areas, and similar pore sizes.

Table 2
Properties of LCO feed.

Density (g/mL) (25 °C)	0.9591
Nitrogen (ppm)	495.6
Sulfur (wt.%)	1.3
Hydrocarbon composition (wt.%)	
Saturates	12.4
Monoaromatics	19.0
Diaromatics	47.0
Polyaromatics	21.6
Distillation (°C)	
0.5 wt.%/10 wt.%	134/214
20 wt.%/30 wt.%	235/254
40 wt.%/50 wt.%	267/282
60 wt.%/70 wt.%	301/318
80 wt.%/90 wt.%	338/362
95 wt.%	377

Table 3
Textural properties of the zeolite beta and catalysts.

Catalyst	MoNi/NB	MoNi/MB	WNi/NB	WNi/MB
Pore volume (mL/g)				
Na-beta	0.86	0.63	0.86	0.63
Treated beta	0.81	0.46	0.81	0.46
Catalyst	0.59	0.51	0.42	0.39
Surface area (m^2/g)				
Na-beta	734	498	734	498
Treated beta	504	432	504	432
Catalyst	220	208	179	165
Average pore sizes (nm)				
Na-beta	4.68	5.05	4.68	5.05
Treated beta	6.43	4.26	6.43	4.26
Catalyst	10.7	9.8	9.4	9.5
Average length of slabs[a] (nm)	6.97	6.30	9.37	16.1
Average number of layers[a]	1.3	2.5	2.4	3.7

[a] Obtained from TEM.

3.2. XRD

The XRD profiles of the oxidic samples are shown in Fig. 1. The characteristic diffraction peaks of γ-Al_2O_3, zeolite beta are marked in the figure. No XRD peaks of any MoO_3, WO_3, or NiO species were identified, which indicates that the molybdenum, tungsten, and nickel species were evenly distributed on the surface of the

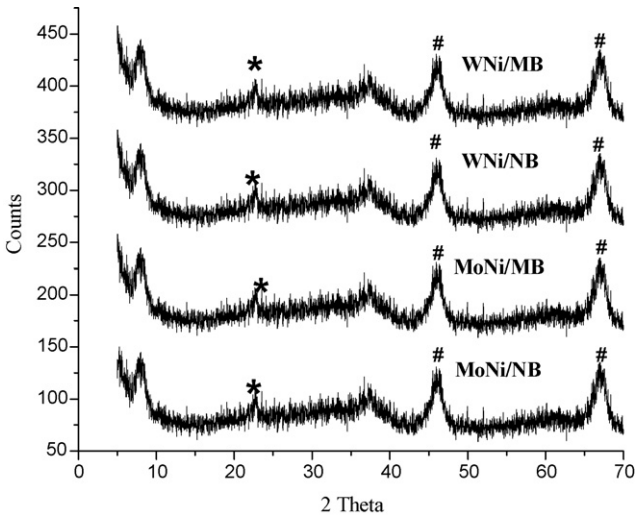

Fig. 1. XRD profiles of MoNi/NB, MoNi/MB, WNi/NB, and WNi/MB. ((*) zeolite beta and (#) γ-Al_2O_3)

support, or metal oxide crystallites were smaller than 4 nm. The characteristic diffraction peaks of γ-Al_2O_3 appeared in all samples, and their intensities were virtually the same for all samples. Compared with the crystallinity of the parent hydrothermally treated zeolite beta, the crystallinities of the zeolite beta on the catalysts were not influenced by the addition of Mo, W, or Ni hydrogenation metals.

3.3. TEM

For Mo-Ni and W-Ni hydrotreating catalysts, Ni-Mo-S and Ni-W-S phases were believed to be the active sites of hydrotreating reactions [20]. Therefore, the catalysts need to be pre-sulfided before use to convert the metal oxides to their corresponding sulfided metals. A direct observation of such sulfided metal structures and distribution with TEM helps to establish the relationship between the properties of the catalysts and their reaction performance. In the Ni-Mo(W)-S model, NiS is considered to be a source of promoter atoms and is located either at the edges in five-fold coordinated sites at $(1\,0\,\bar{1}\,0)$ edge planes of $Mo(W)S_2$ or is present in the alumina lattice [20]. Because of their limited presence in the catalysts and good dispersion, NiS crystals are too small to be directly examined under TEM. The representative TEM images of the four sulfided catalysts are shown in Fig. 2. Energy dispersive X-ray spectrometer (EDX) coupled with TEM is able to identify the species and their composition on the solid surfaces by the characteristic peaks detected. The layered structures on the surfaces of the catalysts had been identified to have the characteristic peaks of MoS_2 or WS_2. The statistical average lengths and numbers of the layers of the MoS_2 and WS_2 slabs are given in Table 3. The distributions of the slab length and the layer number per slab of MoS_2 and WS_2 crystallines are illustrated in Fig. 3. The W-Ni catalysts have much longer average slab length (9.37–16.1 nm) and a greater average number of slab layers (2.4–3.7) than the Mo-Ni catalysts. Compared with the micro-sized zeolites, Mo-Ni/NB has slightly longer slabs and fewer slab layers, while W-Ni/NB has much shorter slabs and fewer slab layers. The WNi catalysts displayed broader distributions of slab length and numbers of layers than MoNi catalysts. MoNi/NB has a similar slab length distribution as MoNi/MB, but its layer number distribution is much narrower, mainly centered in the range 1–2. WNi/NB and WNi/MB show similar broad distributions in slab length and numbers of layers. Their sizes and distributions of MoS_2 and WS_2 are closely related to the surface Si and Al distributions. It has been proved that MoS_2 and WS_2 slabs formed on silica-rich catalyst surfaces are longer and have greater numbers of layers than those formed on aluminium-rich surfaces [21]. The Si in the catalysts is contributed only by the zeolite beta, and the Si/Al ratios of both sizes of zeolites are the same (0.15). During sulfidation, probably due to the different interactions with the surface Si and Al species

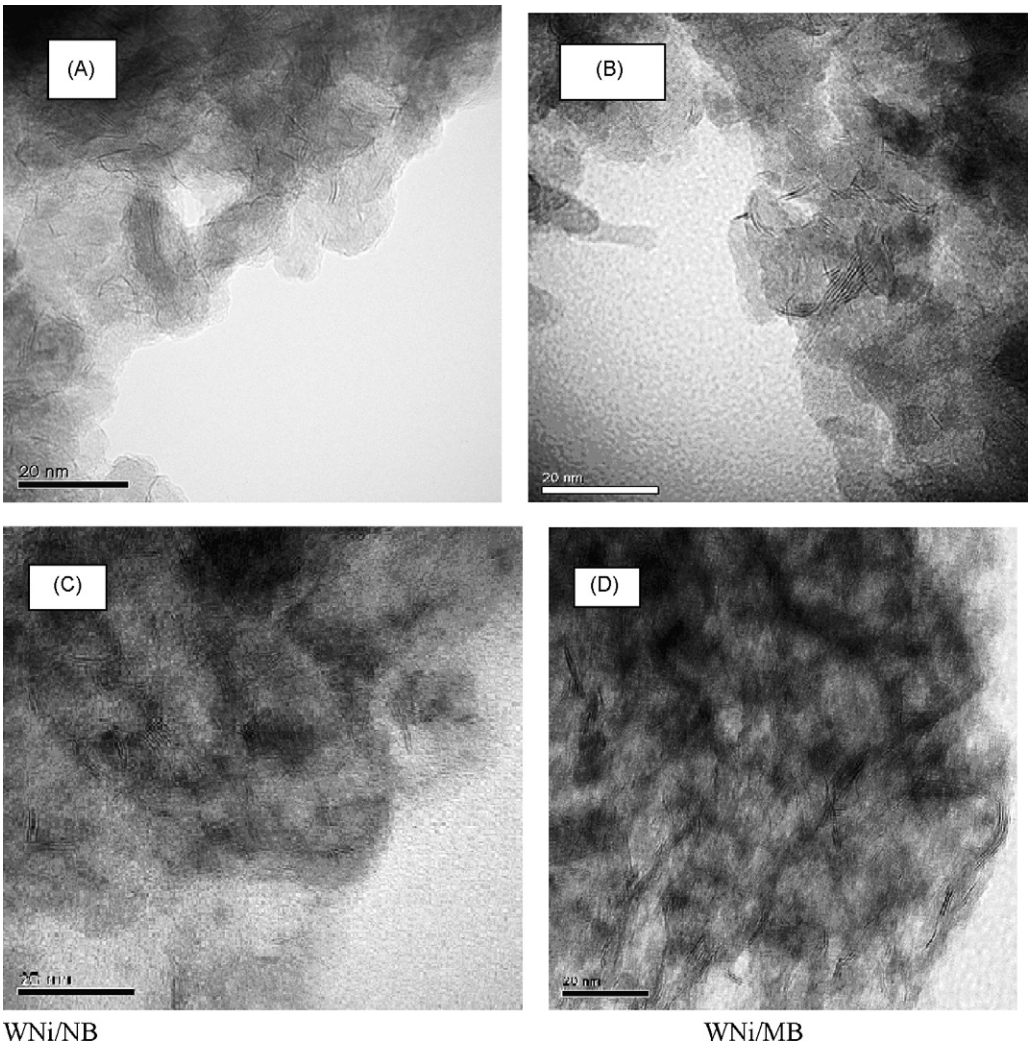

Fig. 2. Representative TEM images of MoNi/NB (A), MoNi/MB (B), WNi/NB (C), and WNi/MB (D). The scale bar in the image is 20 nm long.

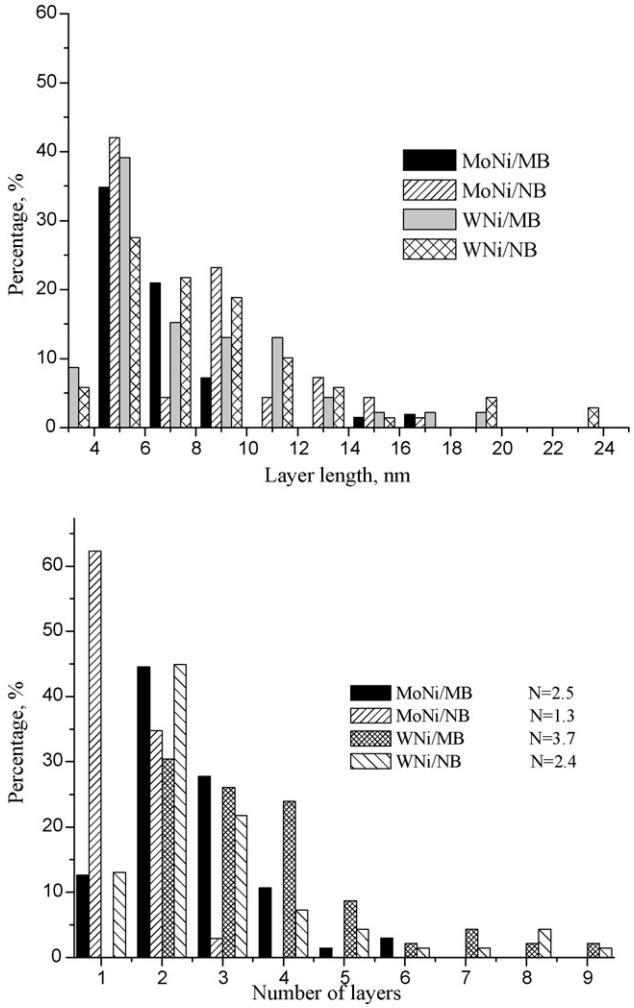

Fig. 3. Distributions of slab length (above) and number of layers (below) of MoS_2 and WS_2 of MoNi/NB, MoNi/MB, WNi/NB, and WNi/MB.

Table 4
Binding energies (BEs) and surface species distributions of oxide and sulfided catalysts.

	MoNi/NB	MoNi/MB	WNi/NB	WNi/MB
Bulk				
Mo/Ni or W/Ni	1.56	1.56	1.55	1.55
Si/Al	0.15	0.15	0.15	0.15
Oxide state				
BE (eV)				
W 4f7			35.6	35.7
W 4f5			37.8	37.8
Mo 3d5	233.0	233.1		
Mo 3d3	236.1	236.3		
Ni 2p3	856.4	856.5	856.4	856.4
Ni 2p1	874.3	874.2	874.4	874.3
Surface species distribution				
Mo/Al + Si or W/Al + Si	0.085	0.077	0.120	0.126
Ni/Al + Si	0.035	0.033	0.041	0.044
Mo/Ni or W/Ni	2.43	2.34	2.93	2.86
Si/Al	0.11	0.14	0.10	0.14
Sulfide state				
BE (eV)				
W 4f7			32.3	32.3
W 4f5			34.3	34.4
Mo 3d5 MoS2	228.7	228.9		
Mo 3d3 MoS2	232.1	232.0		
Mo 3d5 oxy-sulfide	230.6	230.5		
Mo 3d3 oxy-sulfide	233.6	233.6		
Ni 2p3 disulfide	853.4	853.5	853.5	853.5
Ni 2p1 disulfide	871.5	871.4	870.5	870.7
Ni 2p3 NiO	855.4	855.4	855.5	855.7
Ni 2p1 NiO	873.4	873.3	877.3	877.8
S 2p3	161.8	161.9	161.7	161.8
S 2p1	162.9	163.1	163.2	163.2
Surface species distribution				
Mo/Al + Si or W/Al + Si	0.026	0.021	0.052	0.051
Ni/Al + Si	0.025	0.023	0.040	0.041
Mo/Ni or W/Ni	1.05	0.96	1.30	1.25
Si/Al	0.17	0.18	0.15	0.18
S/Mo + Ni or S/W + Ni	1.43	1.32	1.51	1.47

for W and Mo, the surface Si/Al ratios changed and the surface Si/Al ratios of MoNi/NB and WNi/NB became lower than those for MoNi/MB and WNi/MB, especially WNi/NB. The similar Si/Al ratios for MoNi/NB (0.17) and MoNi/MB (0.18) (Table 4) resulted in the similar MoS_2 sizes, while for WNi/NB and WNi/MB, the relatively big difference in Si/Al ratios led to a large variation in WS_2 size.

From TEM, an obvious aggregation was identified for the nano-sized zeolite [22] after hydrothermal treatment. The aggregated particles are formed by loosely jointed 30-nm zeolite crystals. The aggregation results in a totally different distribution and different structures of active sulfided metals. Consequently, the physico-chemical properties and reaction performance of the catalysts containing nano-sized beta particles may be different from those of the catalysts containing "pure" nano- or micro-sized zeolite beta particles.

3.4. XPS

X-ray photoelectron spectra of all calcined (oxidic state) and sulfided catalysts exhibited similar profiles (XPS spectra are not shown). The binding energies (BE) and surface species distributions of the oxidic and sulfided catalysts are summarized in Table 4.

For the Mo-Ni oxide samples, two prominent peaks correspond to the spin-splitting Mo^{6+} $3d_{5/2}$ (BE 233 eV) and Mo^{6+} $3d_{3/2}$ (BE 236 eV) lines of Mo oxide species. The main peaks in the Ni 2p X-ray photoelectron spectra are assigned to the spin-splitting Ni 2p3/2 (BE about 856.4 eV) and Ni 2p1/2 (BE about 874.2 ev) [21]. After sulfidation, the Mo 3d XPS spectra were decomposed into three sets of doublets, corresponding to Mo^{6+}, Mo^{5+}, and Mo^{4+} species. The Mo^{6+}, Mo^{5+}, and Mo^{4+}species species are, respectively, Mo oxide species that were not completely sulfided, the Mo oxy-sulfided species, and MoS_2 (the Ni-Mo-S phases) [23]. The Ni 2p3 XPS spectra of the sulfided catalysts present a relatively intense peak at about 854 eV and a second broad band overlapped partially with the first one, with a BE at around 855.4 eV. The shape of the Ni 2p shows the presence of non-sulfided Ni^{2+} species in all catalysts after sulfidation. The Ni 2p3 peak at 855.4 eV is due to the presence of the non-sulfided Ni^{2+} species. The second Ni 2p3/2 peak at about 853.4 eV, together with the presence of the S 2p3/2 peak at 162 eV, is associated with nickel sulfides [24].

For oxide W-Ni catalysts, the binding energy positions of 37.8 and 35.7 eV are assigned to a doublet peak of W 4f5/2 and W 4f7/2 electrons, respectively [25]. After sulfidation, second doublet peaks appeared at about 34.3 and 32.3 eV, and were assigned to WS_2 phase.

The S 2p spectra of all the sulfided catalysts exhibited one peak at the binding energy value of about 162 eV, which can be assigned to S^{2-} [26]. No other signal was identified around BE 169 eV, indicating that no sulfate species were present, and thus no oxidation of the catalysts occurred during the transfer of the solid from the sulfiding reactor to the XPS chamber.

The similar binding energies of the Mo, W, and Ni species for the two Mo-Ni catalysts and W-Ni catalysts in the oxidic state and sulfided state indicate that there is no significant difference in the interaction between metals (Mo, W or Ni) and supports containing zeolites of both sizes, suggesting that the reduction of zeolite particle sizes did not lead to the change in the metal–support interaction. Although the obvious aggregation was formed in hydrothermally treated nano-sized zeolite beta sample, and zeolite particle size reduction did not cause the change in the interaction, the Mo(W), Ni, Si, and Al distributions on the support were changed. For the oxidic samples, the surface Mo(W)/Ni molar ratios of all the catalysts were higher than for the bulk Mo(W)/Ni, indicating that more Mo or W species were distributed on the surfaces of the catalysts than in the bulk. Only silica and alumina are present on the surface of the supports. It has been verified that Ni species tend to be evenly distributed in the whole support, while the Mo and W species are dominantly distributed in the vacancies on the surface of Al_2O_3 and the zeolite [27–28]. Compared with the Si/Al ratio in the bulk, the supports with lower surface Si/Al ratio zeolite have Al-rich surfaces. During sulfidation, the surface Mo(W)/Si + Al, Ni/Si + Al, and Mo(W)/Ni molar ratios dramatically decreased on the four catalysts, with greater decreases on Mo and W decrease than on Ni species. More Mo or W species are distributed on the nano-sized zeolite catalysts than on the micro-sized zeolite catalysts (Mo or W/Ni ratio 2.43 vs 2.34 for MoNi catalysts and 2.93 vs 2.86 for WNi catalysts). During sulfidation, Ni, W, and Mo species were rearranged [29,30]. The rearrangement caused a significant lateral agglomeration of Mo or W phase to form MoS_2 or WS_2 slabs, and thus a decrease in the apparent coverage of the supports by Mo or W. Interestingly, during sulfidation, the surface Si/Al ratio increased and became even higher than the ratio in the bulk. Compared with Mo-Ni series, the W-Ni series exhibited a bigger difference between nano- and micro-sized zeolite catalysts (0.15 vs 0.18).

The degree of sulfidation of hydrogenation catalyst can be roughly predicted by the atomic ratios of S/[Mo(W) + Ni]. From the S/[Mo(W) + Ni] S/[Mo(W) + Ni] ratios listed in Table 4, it can be noted that the nano-sized zeolite catalysts (MoNi/NB and WNi/NB) had higher S/[Mo(W) + Ni] ratios than the micro-sized zeolite catalysts (MoNi/MB and WNi/MB), which shows that Mo and W on the nano-sized zeolite catalysts seem to be more easily sulfided.

3.5. Reaction performance evaluation

Table 5 summarizes the HDS, HDN, and HDA activities of the four catalysts with the same LCO and under the same reaction conditions. For Mo-Ni series catalysts, HDN and HDS activities of MoNi/NB are exactly the same as those of MoNi/MB, and HDA activity is even lower than that of MoNi/MB. The hydrogenation performance of the Mo-Ni catalyst containing nano-sized zeolite beta is not as expected. However, for W-Ni series catalysts, HDS, HDN, and HDA activities of the catalyst containing nano-sized zeolite beta (WNi/NB) are higher than those of the catalyst containing micro-sized zeolite catalyst (WNi/MB).

As shown in Table 5, after hydrogenation, about 13.3–15.5% of polyaromatics and 22.8–26.4% of diaromatics were converted into monoaromatics on all the catalysts. More polyaromatics and saturate hydrocarbons were produced on WNi catalysts. 1.5% less saturates were produced with MoNi/NB than MoNi/MB; while 1.7% more saturates with WNi/NB than with WNi/MB. Polyaromatics hydrogenation proceeds via successive steps, each of which is a reversible reaction [31]. Based on thermodynamics, the hydrogenation reactivity of aromatics decreases in the following order: polyaromatics > biaromatics > monoaromtics [31]. The hydrogenation of the monoaromatics is difficult and only attained when the temperature is higher than approximately 673 K with non-noble metal catalysts [32]. The monoaromatics are still low cetane number components. To significantly increase the cetane number of diesel fuel, high activity ring opening catalysts need be developed.

Table 5
Reaction performance of the four catalysts in LCO hydrotreating (reaction conditions: temperature 648 K; initial pressure 6.8 MPa, duration 2 h).

Sample	MoNi/NB	MoNi/MB	WNi/NB	WNi/MB
Density (15.6 °C) (g/mL)	0.9131	0.9123	0.9090	0.8968
Total nitrogen (ppm)	37.32	37.12	1.45	22.80
Total sulfur (ppm)	889.4	889.2	777.4	977.6
Hydrocarbon distribution (wt%)				
Saturates	22.1	23.6	27.2	25.5
Monoaromatics	45.6	44.4	45.0	47.8
Diaromatics	24.2	23.7	20.8	20.6
Polyaromatics	8.1	8.3	7.0	6.1
HDN (%)	92.47	92.51	97.08	95.40
HDS (%)	93.16	93.16	94.02	92.48
HDA (%)	9.7	11.2	14.70	13.10
Liquid yield (wt%)	92.9	92.1	91.6	90.8
SIMDIS (°C)				
0.5%	125.0	119.6	103.5	115.0
5%	203.0	197.6	178.5	193.0
10%	220.0	214.6	201.5	210.0
20%	239.5	234.1	224.0	229.5
30%	255.0	249.6	236.5	245.0
40%	268.0	262.6	252.0	258.0
50%	283.0	277.6	266.0	273.0
60%	298.5	293.1	283.0	288.5
70%	316.0	310.6	301.5	306.0
80%	337.5	332.1	322.5	327.5
90%	366.0	360.6	351.5	356.0
95%	389.5	384.1	375.0	379.5
99.5%	523.0	517.6	501.5	513.0

For both series of catalysts, the nano-sized zeolite catalysts exhibited a higher liquid yield. It has been proved that HDS promotional effects of Ni in Mo- and W-based catalysts are related to the presence of structures similar to Ni-Mo-S or Ni-W-S. The lateral dimensions of the MoS_2 or WS_2 structure are important parameters in determining the reaction performance of hydrotreating catalysts [33] because the corners and edges of the Mo(W)S_2 slabs are believed to be the active sites of hydrogenation. The more corners and edges the Mo(W)S_2 slabs can provide, the greater the hydrogenation activity of the catalyst. For a given metal content, there is an optimal length and number of layers in each slab to offer the greatest number of metal active sites. Obviously, the different interactions of W and Mo with the support resulted in the various WS_2 and MoS_2 sizes and size distributions. Apparently, W-Ni supported on nano-sized zeolite beta is more favorable in hydrotreating LCO than supported on micro-sized zeolite beta. Considering the similar pore structures (Table 3, the specific surface areas of WNi catalysts were even lower than those of MoNi ones) and similar metal-and-support interactions between MoNi and WNi catalysts (Table 4), the difference in catalyst performances is probably mainly due to the variation in Mo(W)-Ni-S structures and sizes. The studies on the correlation between the Mo(W)-Ni-S structures and hydrogenation activity are under conducting. Besides the non-optimal sizes of MoS_2, the lower activity of MoNi/NB is probably also caused by the aggregation of nano-sized zeolite particles. An approach to the prevention of aggregation is being developed.

A slightly higher liquid yield (0.8 wt.%, Table 5) was achieved by the two nano-sized zeolite catalysts. As the experimental error for the liquid yield was 0.01 wt.% (the error resulted from weighing samples), 0.8 wt.% was a considerable difference. The higher liquid

yield means more diesel fuel can be produced from the same amount of feed. The 0.8-wt% increase could add 8000 t/y of extra diesel fuel to production from a 1-Mt/y hydrotreater. The aggregation of a considerable amount of nano-sized zeolite during calcination and hydrothermal treatment altered the surface Mo(W) Ni distribution, and subsequently the number of active hydrogenation sites. However, because the aggregated particles were formed by the loosely jointed 30-nm nano-sized zeolite crystals, the inter-particle space was still much greater than in micro-sized zeolite, and the diffusion of the feed and product molecules is still easier and quicker. Due to the short diffusion path and more active sites located on the outer surface, secondary cracking of product molecules is avoided to some extent, and thus less gas product is produced and higher liquid yield is obtained by the nano-sized zeolite catalysts.

4. Conclusions

Comparisons of catalysts containing micro-sized and nano-sized zeolite beta particles identified no significant differences in pore structure, crystalline phases, or interactions between metals and supports. The W-Ni catalysts presented much longer average slab lengths and greater average numbers of slab layers than the Mo-Ni catalysts. The Mo-Ni nano-sized zeolite catalyst had slightly longer slabs and fewer slab layers than the micro-sized zeolite, while W-Ni nano-sized zeolite showed much shorter slabs and fewer slab layers.

The HDN and HDS activities of the Mo-Ni nano-sized zeolite catalyst were the same as those of the micro-sized zeolite catalysts, and the HDA activity was lower. For W-Ni series catalysts, the HDS, HDN, and HDA activities of the catalyst containing nano-sized zeolite beta were higher than those of the micro-sized zeolite catalyst. The two nano-sized zeolite catalysts gave higher liquid yields in hydrotreating LCO.

References

[1] C. Song, Catal. Today 86 (2003) 211.
[2] E. Lecrenay, K. Sakanishi, I. Mochida, Catal. Today 39 (1997) 13.
[3] I. Isoda, S. Nagao, X. Ma, Y. Korai, I. Mochida, Energy Fuels 10 (1996) 1078.
[4] S. Bendezu, R. Cid, J.L.G. Fierro, A.L. Agudo, Appl. Catal. A: Gen. 197 (2000) 47.
[5] F. Bataille, J.L. Lemberton, G. Perot, P. Leyrit, T. Cseri, N. Marchal, S. Kasztelan, Appl. Catal. A 220 (2001) 191.
[6] C. Leyva, M.S. Rana, F. Trejo, J. Ancheyta, Ind. Eng. Chem. Res. 46 (2007) 7448.
[7] J. Weitkamp, Solid State Ionics 131 (2000) 175.
[8] M.V. Landau, L. Vradman, V. Valtchev, J. Lezervant, E. Liubich, M. Talianker, Ind. Eng. Chem. Res. 42 (2003) 2773.
[9] S.M. Auerbach, K.A. Carrado, P.K. Dutta, Handbook of Zeolite Science and Technology, Marcel Dekker Inc., 2003,, p. 130.
[10] M.A. Camblor, A. Corma, A. Martinez, V. Martinez-Soria, S. Valencia, J. Catal. 179 (1998) 537.
[11] J. Weitkamp, Solid State Ionics 131 (2000) 175–188.
[12] E.F.S. Aguiar, M.L.M. Valle, M.P. Silva, D.F. Silvat, Zeolites 15 (1995) 620.
[13] M. Yamamura, K. Chaki, T. Wakatsuki, H. Okado, K. Fujimoto, Zeolites 14 (1994) 643.
[14] R. Loenders, P.A. Jacobs, J.A. Martens, J. Catal. 176 (1998) 545.
[15] M.A. Arribas, A. Martinez, Catal. Today 65 (2001) 117.
[16] G. Harvey, G. Binder, R. Prins, Stud. Surf. Sci. Catal. 94 (1995) 397.
[17] H. Topsoe, B.S. Clausen, F.E. Massoth, Hydrotreating catalysis, pp. 22.
[18] L. Ding, Y. Zheng, Z. Zhang, Z. Ring, C. Jin, Micropor. Mesopor. Mater. 94 (2006) 1–8.
[19] M.A. Camblor, A. Corma, S. Valencia, Micropor. Mesopor. Mater. 25 (1998) 89.
[20] H. Topsoe, B.S. Clausen, F.E. Massoth, Hydrotreating catalysis, pp. 31.
[21] L. Ding, Y. Zheng, Z. Zhang, Z. Ring, J. Chen, Appl. Catal. A 319 (2007) 25.
[22] L. Ding, Y. Zheng, Z. Zhang, Z. Ring, J. Chen, Micropor. Mesopor. Mater. 101 (2007) 432.
[23] D. Li, T. Sato, M. Imamura, H. Shimada, A. Nishijima, J. Catal. 170 (1997) 357.
[24] B. Pawelec, L. Daza, J.L.G. Fierro, J.A. Anderson, Appl. Catal. A 145 (1996) 307.
[25] L. Salvati, J.L. Makovsky, J.M. Stencel, F.R. Brown, D.M. Hercules, J. Phys. Chem. 85 (1981) 3700.
[26] S. Bendez, R. Cid, J.L.G. Fierro, A.L. Agudo, Appl. Catal. A 197 (2000) 47.
[27] D. Li, A. Nishijima, D.E. Morris, G.D. Guthrie, J. Catal. 188 (1999) 111.
[28] Y.W. Li, X.Y. Pang, B. Delmon, J. Mol. Catal. A: Chem. 169 (2001) 259.
[29] N.Y. Topsoe, H. Topsoe, J. Catal. 139 (1993) 631.
[30] N.Y. Topsoe, H. Topsoe, J. Catal. 139 (1993) 641.
[31] B.H. Cooper, B.B.L. Donnis, Appl. Catal. A 137 (1996) 203–223.
[32] M. Bouchy, P. Dufresne, S. Kasztelan, Ind. Eng. Chem. Res. 31 (1992) 2661.
[33] S. Eijsbouts, J.J.L. Heinerman, H.J.W. Elzerman, Appl. Catal. A 105 (1993) 53.